Multi-turbine Cooperative Frequency Regulation Control for Wind Farms Considering Torque-limited Inertial Control Power Characteristics

Wei Gu, Minghui Yin, Qiang Li, Yaran Li, Zaiyu Chen, and Qun Li

***Abstract*—Torque-limited inertial control (TLIC) offers advantages of stabilizing wind turbine (WT) operation and mitigating secondary frequency dip. When large-scale wind farm (WF) clusters simultaneously employ TLIC to provide power support, unnecessary frequency recoil (FR) phenomenon may occur, persistently degrading the frequency regulation performance. To address this issue, the paper analyzes the frequency response characteristic under TLIC method, and derives the conditions for FR under simultaneous and immediate support and simultaneous and delayed support, with the latter exhibiting more pronounced FR effects. The root cause of FR is identified as excessive power increments. Hence, the multi-turbine cooperative frequency regulation control method for WFs considering the TLIC power characteristics is proposed. By sequentially activating TLIC among WTs, the excessive power increment from simultaneous support is mitigated, and the gradual power reduction of the engaged WTs can be compensated. Experimental validation is conducted based on the test bench of wind-integrated power system, which demonstrates that the proposed method effectively avoids FR and further enhances the frequency nadir.**

***Index Terms*—Wind farm (WF), wind turbine (WT), torque-limited inertial control (TLIC), frequency regulation control, frequency recoil (FR).**

I. Introduction

With the continuous increase of the wind turbine (WT) installed capacity, the grid-connection method through power electronic converters significantly reduces the equivalent inertia of the power system, making the frequency stability problem more prominent [1]-[4]. This urgently requires wind power to have the ability of short-term frequency support control (SFSC) [5]-[7].

According to different criteria for setting power commands, the existing SFSC methods can be divided into the following three categories. ① The SFSC methods based on the relationship between the power and frequency simulate the power output characteristics of synchronous generators (SGs) [8]-[11], such as virtual inertial control, droop control, and comprehensive inertial control. ② The SFSC methods based on the relationship between the power and time set the power command as a constant value [12], [13] or the optimal support power trajectory [14], [15]. ③ The SFSC methods based on the relationship between the power and WT rotor speed set the relationship as linear [16]-[18], cubic [19], or satisfying Gaussian distribution characteristics [20], and due to the strong operation stability of WT and the ability to avoid secondary frequency dips (SFDs) [16]-[18], this method is the main research object of this paper.

The existing research primarily focuses on the coordination among WTs with different operation states, primarily focusing on two aspects. The first is the differentiated setting of WT frequency regulation parameters under different operation states, aiming to maximize frequency regulation capability utilization while ensuring stable wind farm (WF) operation. The second is the coordinated deactivation mechanisms for WTs, preventing severe SFDs caused by the abrupt power reduction when all WTs simultaneously exit the frequency regulation stage.

The operation states of WTs within a WF varies significantly due to their exposure to different wind speeds. Differentiating the frequency regulation control parameters for individual WTs is key to balancing WT operation stability with frequency regulation performance [21]-[23]. Reference [23] establishes WT frequency regulation capability metrics and feasible regions for droop and virtual inertial coefficients, and assesses frequency regulation capabilities under different wind speeds. On this basis, WT-specific frequency regulation parameters are configured to fully exploit frequency regulation potential while ensuring stable operation of both individual WTs and the entire WF. This method enhances adaptability to wind speed while avoiding inappropriate parameters that could trigger WT rotor speed protection, thereby preventing SFDs [24]. Under the trend toward larger WTs, the

Manuscript received: June 14, 2025; revised: September 26, 2025; accepted: November 20, 2025. Date of CrossCheck: November 20, 2025. Date of online publication: December 9, 2025.

This work was supported by the National Key Research and Development Program of China (No. 2023YFB4204700).

W. Gu, M. Yin (corresponding author), and Z. Chen are with the School of Automation, Nanjing University of Science and Technology, Nanjing, China (e-mail: dafenguwei@126.com; ymhui@njust.edu.cn; zaiyu.chen@njust.edu.cn).

Q. Li, Y. Li, and Q. Li are with the State Grid Jiangsu Electric Power Co., Ltd. Research Institute, Nanjing, China (e-mail: 35830342@qq.com; yaran.li@unswalumni.com; qun_li@sina.com).

DOI: 10.35833/MPCE.2025.000547

loads of WTs have been focused on. Hence, suppressing loads on critical mechanical components such as gearboxes and drive trains during the frequency support phase has become one of the primary objectives in optimizing the settings of frequency regulation control parameters [25], [26].

Regarding the coordinated exit mechanism of WT SFSC method, the setting of frequency regulation control parameters or support power is determined based on the extent of kinetic energy release across different WTs. By slowing down the kinetic energy release rate as rotor speed decreases and gradually reducing support power, this method enables a smooth transition for WTs out of the frequency support stage [24], [27]. Among these, [28] introduces a collaborative control coefficient to coordinate the allocation and compensation of frequency regulation auxiliary power among WTs, thereby achieving simultaneous frequency support and rotor speed recovery. In contrast, [21] and [29] first develop a smooth transition process for WTs moving from the frequency support stage to the rotor speed recovery stage, which prevents abrupt power reduction in individual WT and avoids SFDs caused by simultaneous power decrease across all WTs through sequential exit of WFs [21], [30], [31]. For the grouped exit method, a mechanism is designed based on the torque-limited inertial control (TLIC) method that introduces time delays between the instants of rotor speed recovery startup across WT groups [32].

However, with the rising penetration of wind power, the concurrent activation of WT SFSC methods across WF clusters may induce a sudden surge in power injection, triggering a frequency recoil (FR) phenomenon and adversely affecting the subsequent frequency response. This ultimately limits the improvement effect in the frequency nadir (FN). To address this issue, this paper analyzes the frequency response characteristics of power systems with wind power participating through TLIC. Specifically, it derives the FR occurrence conditions under two methods: simultaneous and immediate support (SIIS) and simultaneous and delayed support (SIDS), and reveals that the latter exhibits more pronounced FR.

Then, considering the synchronized rise and fall characteristic of TLIC power, the multi-turbine cooperative frequency regulation control method is proposed. By monitoring the frequency dynamic and detecting whether the FN is reached, the sequential activation of TLIC across WTs is implemented. This method not only mitigates the excessive power surge but also compensates for the gradually decreasing electric power of already activated WTs. Finally, experimental validation is conducted on the test bench of wind-integrated power system. Results demonstrate that the proposed method effectively avoids the FR during WF clusters participating in the frequency regulation, and further elevates the FN.

The remainder of the paper is organized as follows. The model of wind power participating in the frequency regulation is described in Section II. In Section III, the FR under simultaneous support is introduced. Section IV proposes multi-turbine cooperative frequency regulation control method of WFs. In Section V, the proposed method is verified by experiments performed on the test bench of the wind-integrated power system. Conclusions are drawn in Section VI.

II. Model of Wind Power Participating in Frequency Regulation

The TLIC method, known for strong operation stability for WTs [16]-[18], has emerged as a research hotspot in existing studies and serves as the focus of this paper. Accordingly, this section introduces the WF model employing the TLIC method and the power system frequency response model involving TLIC participation. Notably, given that electromagnetic dynamics operate at a much faster timescale than electromechanical dynamics [33], this paper primarily focuses on the latter aligned with the frequency response timescale. It is assumed that the generator control can rapidly and accurately respond to the torque commands.

A. Model of TLIC-based WT and WF

Normally, WTs operate in the maximum power point tracking (MPPT) control mode. When a sudden load surge or generator tripping event occurs, WTs switch from MPPT mode to TLIC mode to release the kinetic energy of the wind rotor, so as to provide the additional power support for maintaining the frequency stability. The TLIC method is illustrated in Fig. 1, showing the transition process (blue curves) of WT operation points under the TLIC method.

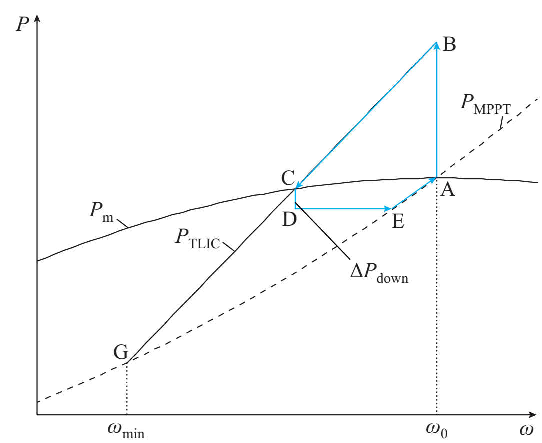

Fig. 1. Illustration of TLIC method.

1) Frequency Support Stage

When the frequency event occurs, the TLIC method increases the electric power of the WT from initial $P_{MPPT}(\omega_0)$ to higher $P_{TLIC}(\omega_0)=T_{elim}\omega_0$, i. e., the WT operates from points A to B, where P_{MPPT} is the optimal power corresponding to MPPT method; ω_0 is the initial rotor speed corresponding to point A; P_{TLIC} is the optimal power corresponding to TLIC method; and T_{elim} is the maximum electrical torque. Then, the power command is set based on rotor speed according to (1) and (2). The WT subsequently operates along the predefined power curve (points B to C). During this process, the electric power is always larger than the aerodynamic power, the WT keeps operating in a decelerating mode, so as to release the kinetic energy of wind rotor to support the active power balance for the power system.

$$P_{TLIC}(\omega)=K_{P,\omega}(\omega-\omega_{min})+P_{MPPT}(\omega_{min}) \tag{1}$$

$$K_{P,\omega}=\frac{T_{\mathrm{elim}}\omega_0-P_{\mathrm{MPPT}}(\omega_{\min})}{\omega_0-\omega_{\min}} \tag{2}$$

where ω is the rotor speed; $K_{P,\omega}$ is the slope coefficient of the TLIC method; and $\omega_{\min}$ is the minimum rotor speed corresponding to point G.

$$\begin{cases} P_{\mathrm{MPPT}}(\omega)=K_{\mathrm{opt}}\omega^3 \\ K_{\mathrm{opt}}=\dfrac{0.5\rho\pi R^5 C_{\mathrm{pmax}}}{\lambda_{\mathrm{opt}}^3} \end{cases} \tag{3}$$

where K_{opt} is the optimal power coefficient; ρ is the air density; R is the radius of the wind rotor; C_{pmax} is the maximum power coefficient; and λ_{opt} is the optimal tip speed ratio when the pitch angle is 0°.

2) Rotor Speed Recovery Stage

When WT decelerates to point C, the output power equals the captured aerodynamic power, allowing it to stably operate at this equilibrium point. Through slightly reducing the electric power command by ΔP_{down} from the stable equilibrium point C to point D, WT accelerates along the D-E curve, so as to realize the rotor speed recovery. Once the WT accelerates to point E, it switches back to the MPPT mode, thereby completing rotor speed recovery after frequency support.

$$P_{\mathrm{rec}}=P_{\mathrm{TLIC}}(\omega_{\mathrm{C}})-\Delta P_{\mathrm{down}} \tag{4}$$

$$\omega_{\mathrm{E}}=\sqrt[3]{\frac{P_{\mathrm{rec}}}{K_{\mathrm{opt}}}} \tag{5}$$

where P_{rec} is the recovery power from point D to point E; ω_{E} is the rotor speed corresponding to point E, which is the intersection point between the D-E curve and the MPPT curve; and ω_{C} is the rotor speed corresponding to point C.

For a WF, the total output power of WF P_{W} during the frequency support stage is the sum of the electric power outputs from each WT.

$$P_{\mathrm{W}}=\sum_{i=1}^{N}P_{\mathrm{TLIC}i}(\omega_i) \tag{6}$$

where N is the number of WTs in WF; and i denotes the i^{th} WT.

B. Power System Frequency Response Model

The complete frequency regulation process includes stages such as inertial response, primary frequency control, and secondary frequency control. This paper primarily focuses on the frequency dynamic and the FN during the first two stages. Based on the WT and WF power models under TLIC method, the single-machine equivalent model for frequency response in a wind-integrated power system is illustrated in Fig. 2 [34], where P_{W0} is the initial output power of WF. The remaining variables are explained in the following text.

The WF power acts as a positive power disturbance, while the load power serves as a negative power disturbance.

$$\begin{cases} \Delta f(s)=\dfrac{1}{2Hs+D}\left(\Delta P_{\mathrm{W}}(s)+\Delta P_{\mathrm{M}}(s)-\Delta P_{\mathrm{L}}(s)\right) \\ \Delta P_{\mathrm{M}}(s)=\dfrac{K_{\mathrm{m}}(1+F_{\mathrm{H}}T_{\mathrm{R}}s)}{R_{\mathrm{g}}(1+T_{\mathrm{R}}s)}\Delta f(s) \end{cases} \tag{7}$$

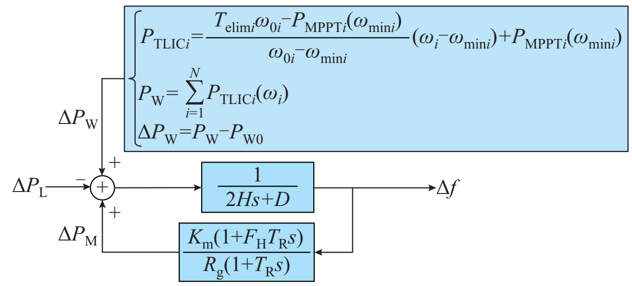

Fig. 2. Single-machine equivalent model for frequency response in a wind-integrated power system.

$$\Delta f(s)=\frac{R_{\mathrm{g}}(1+T_{\mathrm{R}}s)}{(2Hs+D)R_{\mathrm{g}}(1+T_{\mathrm{R}}s)-K_{\mathrm{m}}(1+F_{\mathrm{H}}T_{\mathrm{R}}s)}\left(\Delta P_{\mathrm{W}}(s)-\Delta P_{\mathrm{L}}(s)\right)=G(s)\left(\Delta P_{\mathrm{W}}(s)-\Delta P_{\mathrm{L}}(s)\right) \tag{8}$$

where ΔP_{M} is the mechanical power increment of the SG; ΔP_{W} is the electric power increment of the WF; ΔP_{L} is the load power increment; H is the inertia constant of the equivalent system; D is the damping factor; R_{g} is the governor regulation factor; K_{m} is the mechanical power gain factor; F_{H} is the fraction of total power generated by the high pressure WT; T_{R} is the reheat time constant; Δf is the frequency deviation of the power system; and $G(s)$ is the transfer function of the power system.

According to the superposition theorem for the linear system, by applying the inverse Laplace transform to (8), the time-domain expression of the frequency response can be obtained, which is the superposition of the frequency response components induced separately by load power and wind power.

$$\Delta f(t)=\Delta f_{\mathrm{W}}(t)-\Delta f_{\mathrm{L}}(t) \tag{9}$$

where Δf_{W} is the frequency response component under the wind power activation; Δf_{L} is the frequency response component under the load surge power activation; and t denotes the time.

For the load surge event, $\Delta f_{\mathrm{L}}(t)$ is described as:

$$\Delta f_{\mathrm{L}}(t)=\Delta P_{\mathrm{L}}h_{\mathrm{step}}(t) \tag{10}$$

where h_{step} is the unit step response of G [34].

$$h_{\mathrm{step}}(t)=r\left(1+\alpha \mathrm{e}^{-\xi\Omega_{\mathrm{n}}t}\sin(\Omega_{\mathrm{r}}t+\phi)\right) \tag{11}$$

$$\begin{cases} r=\dfrac{R_{\mathrm{g}}}{DR_{\mathrm{g}}+K_{\mathrm{m}}} \\ \Omega_{\mathrm{n}}=\sqrt{\dfrac{DR_{\mathrm{g}}+K_{\mathrm{m}}}{2HR_{\mathrm{g}}T_{\mathrm{R}}}} \\ \xi=\dfrac{2HR_{\mathrm{g}}+\left(DR_{\mathrm{g}}+K_{\mathrm{m}}F_{\mathrm{H}}\right)T_{\mathrm{R}}}{2\left(DR_{\mathrm{g}}+K_{\mathrm{m}}\right)}\Omega_{\mathrm{n}} \\ \Omega_{\mathrm{r}}=\Omega_{\mathrm{n}}\sqrt{1-\xi^2} \\ \alpha=\sqrt{\dfrac{1-2\xi T_{\mathrm{R}}\Omega_{\mathrm{n}}+T_{\mathrm{R}}^2\Omega_{\mathrm{n}}^2}{1-\xi^2}} \\ \phi=\arctan\left(\dfrac{\Omega_{\mathrm{r}}T_{\mathrm{R}}}{1-\xi\Omega_{\mathrm{n}}T_{\mathrm{R}}}\right)-\arctan\left(\dfrac{\sqrt{1-\xi^2}}{-\xi}\right) \end{cases} \tag{12}$$

The variables in (12) are intermediate coefficients for power system frequency response model. The TLIC power of a single WT is simplified into the two-segment form [16], as illustrated by the dashed line L-M-N in Fig. 3 and (13).

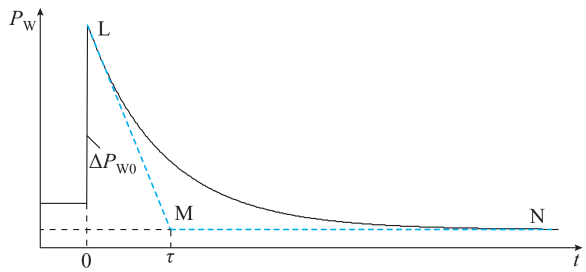

Fig. 3. Simplified form of P_W.

$$\Delta P_W(t) = \Delta P_{W0} u(t) + K_{P,t} t u(t) - K_{P,t}(t-\tau) u(t-\tau) \tag{13}$$

where ΔP_{W0} is the initial power increment of TLIC method; $u(\cdot)$ is the step function; $K_{P,t}$ is the power curve slope on the time domain; and τ is the time that the power decreases from the initial value to the steady value at point N. The corresponding frequency response is given by:

$$\Delta f_W(t) = \Delta P_{W0} h_{step}(t) + K_{P,t} h_{ramp}(t) u(t) - K_{P,t} h_{ramp}(t-\tau) u(t-\tau) \tag{14}$$

where h_{ramp} is the unit slope response of G [16].

$$h_{ramp}(t) = rt + \frac{r\alpha}{\xi^2 \Omega_n^2 + \Omega_r^2}\left(\xi \Omega_n \sin\phi + \Omega_r \cos\phi\right) - \frac{r\alpha}{\xi^2 \Omega_n^2 + \Omega_r^2} \cdot e^{-\xi \Omega_n t}\left(\xi \Omega_n \sin\left(\Omega_r t + \phi\right) + \Omega_r \cos\left(\Omega_r t + \phi\right)\right) \tag{15}$$

III. FR Under Simultaneous Support

When a sudden load surge event occurs, if all WTs in the WF clusters simultaneously activate the TLIC method, the abrupt power surge may induce the unnecessary FR phenomenon. This disrupts the subsequent frequency response dynamics and limits the effectiveness of WF participating in the frequency regulation. Hence, this section provides a simulation-based case study of the FR and derives the conditions under which simultaneous activation causes the FR.

A. FR Phenomenon

The simulation model contains five WTs and the single-machine equivalent model with the parameters referred from [34], which is shown in Fig. 4. The simulation scenario is set as follows. The wind speed for all WTs is 10 m/s, the wind power penetration is 25%, and the load increases by 300 kW at the moment of 300 s. The simulation results of Δf, P_W, P_M, and system unbalanced power ΔP under SIIS, SIDS, and no support (NoS) are illustrated in Fig. 5.

When the WF participates in the frequency regulation via SIIS or SIDS, its power surge exceeds the system power deficit, resulting in a positive power imbalance, which induces the FR. With the increase of delay time, the FR exhibits an increasing trend. Due to the solid power increment of the WF, the unbalanced power is reduced with the time, so the WF increment power will induce more redundant power, which causes a more evident FR. Under the three methods, the FN statistics are 0.6602 Hz, –0.6587 Hz, and –0.6043 Hz, respectively. It can be referred that simultaneous activation of TLIC fails to significantly improve the frequency regulation performance, as evidenced by the marginal difference in the FN between SIIS and NoS as well as SIDS and NoS.

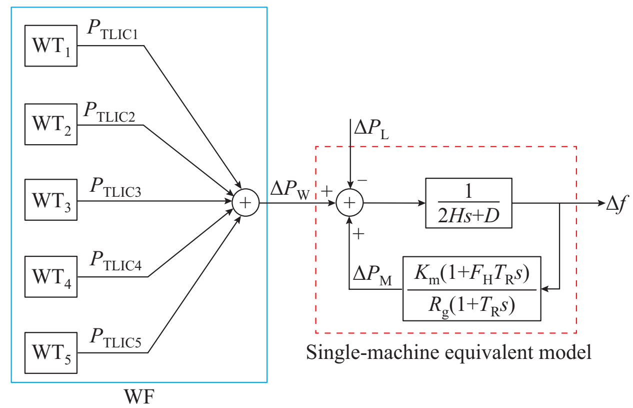

Fig. 4. Network topology for simulation model.

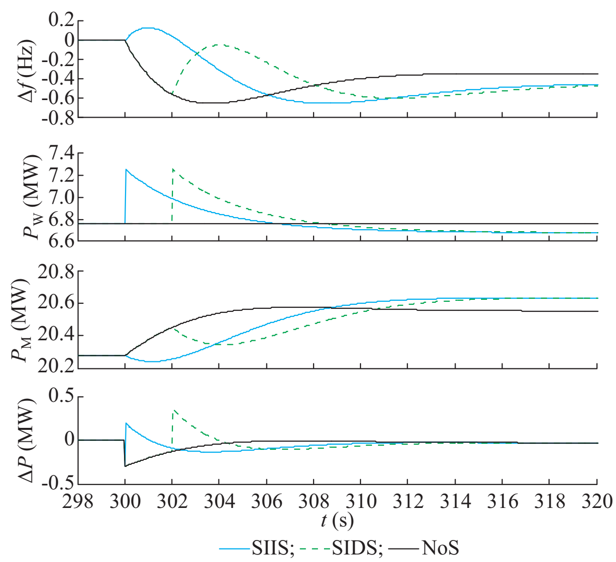

Fig. 5. Simulation results of Δf, P_W, P_M, and ΔP.

B. Occurrence Conditions of FR

Assume that all N WTs in the WF have identical initial operation states (e.g., wind speed and rotor speed) and employ identical TLIC parameters. When all WTs delay the activation of the TLIC method by a time period t_d, $\Delta P_W(t)$ transitions from (13) to (16).

$$\Delta P_W(t) = \Delta P_{W0} u(t-t_d) + K_{P,t}(t-t_d) u(t) - K_{P,t}(t-t_d-\tau) u(t-t_d-\tau) \tag{16}$$

Therefore, the time-domain expression of the frequency response component under the delayed TLIC power is given by:

$$\Delta f_W(t) = \Delta P_{W0} h_{step}(t-t_d) + K_{P,t} h_{ramp}(t-t_d) u(t-t_d) - K_{P,t} h_{ramp}(t-t_d-\tau) u(t-t_d-\tau) \tag{17}$$

When N WTs in the WF simultaneously delay the activation of the TLIC method following a frequency event, the time-domain expression of the frequency response component is given by:

$$N\Delta f_{\mathrm{W}}(t)=N\Delta P_{\mathrm{W0}}h_{\mathrm{step}}(t-t_{\mathrm{d}})+NK_{P,t}h_{\mathrm{ramp}}(t-t_{\mathrm{d}})\cdot u(t-t_{\mathrm{d}})-NK_{P,t}h_{\mathrm{ramp}}(t-t_{\mathrm{d}}-\tau)u(t-t_{\mathrm{d}}-\tau) \tag{18}$$

By performing a derivative operation on (18), the rate of change of the frequency under the influence of delayed TLIC power can be derived as:

$$N\Delta f_{\mathrm{W}}'(t)=\begin{cases}0 & t\le t_{\mathrm{d}}\\ N\Delta P_{\mathrm{W0}}h'_{\mathrm{step}}(t-t_{\mathrm{d}})+NK_{P,t}h_{\mathrm{step}}(t-t_{\mathrm{d}}) & t_{\mathrm{d}}<t\le t_{\mathrm{d}}+\tau\\ N\Delta P_{\mathrm{W0}}h'_{\mathrm{step}}(t-t_{\mathrm{d}})+NK_{P,t}h_{\mathrm{step}}(t-t_{\mathrm{d}})-NK_{P,t}h_{\mathrm{step}}(t-t_{\mathrm{d}}-\tau) & t>t_{\mathrm{d}}+\tau\end{cases} \tag{19}$$

Therefore, the rate of change of the frequency response under the combined effects of a sudden load power surge and simultaneously-delayed TLIC power is given by:

$$\Delta f'(t)=N\Delta f_{\mathrm{W}}'(t)-\Delta f_{\mathrm{L}}'(t)=\begin{cases}-\Delta P_{\mathrm{L}}h'_{\mathrm{step}}(t) & t\le t_{\mathrm{d}}\\ N\Delta P_{\mathrm{W0}}h'_{\mathrm{step}}(t-t_{\mathrm{d}})+NK_{P,t}h_{\mathrm{step}}(t-t_{\mathrm{d}})-\Delta P_{\mathrm{L}}h'_{\mathrm{step}}(t) & t_{\mathrm{d}}<t\le t_{\mathrm{d}}+\tau\\ N\Delta P_{\mathrm{W0}}h'_{\mathrm{step}}(t-t_{\mathrm{d}})+NK_{P,t}h_{\mathrm{step}}(t-t_{\mathrm{d}})-NK_{P,t}h_{\mathrm{step}}(t-t_{\mathrm{d}}-\tau)-\Delta P_{\mathrm{L}}h'_{\mathrm{step}}(t) & t>t_{\mathrm{d}}+\tau\end{cases} \tag{20}$$

It can be observed from (19) and (20) that at the moment of the WTs participating in the frequency regulation with TLIC method, $h_{\mathrm{step}}(0^+)$ is very small and nearly equals 0, which can be neglected, and the change direction of the frequency is determined mainly by $N\Delta P_{\mathrm{W0}}h'_{\mathrm{step}}(t_{\mathrm{d}}^+-t_{\mathrm{d}})-\Delta P_{\mathrm{L}}h'_{\mathrm{step}}(t_{\mathrm{d}}^+)$. The superscript $^+$ indicates a value that is marginally greater than the baseline measurement. That is to say, if all WTs in the WF are delayed in activating the TLIC method, and the resulting electric power increment along with the sudden load increase satisfies the condition specified in (21), the FR phenomenon will occur.

$$N\Delta P_{\mathrm{W0}}h'_{\mathrm{step}}(t_{\mathrm{d}}^+-t_{\mathrm{d}})>\Delta P_{\mathrm{L}}h'_{\mathrm{step}}(t_{\mathrm{d}}^+) \tag{21}$$

Considering different wind speeds and rotor speeds among WTs and the delay time, the occurrence conditions of FR under SIIS and SIDS are listed in Table I.

TABLE I
OCCURRENCE CONDITIONS OF FR UNDER SIIS AND SIDS

State	FR under SIIS	FR under SIDS
Same initial operation states	$N\Delta P_{\mathrm{W0}}>\Delta P_{\mathrm{L}}$	$N\Delta P_{\mathrm{W0}}h'_{\mathrm{step}}(t_{\mathrm{d}}^+-t_{\mathrm{d}})>\Delta P_{\mathrm{L}}h'_{\mathrm{step}}(t_{\mathrm{d}}^+)$
Different initial operation states	$\sum_{i=1}^{N}\Delta P_{\mathrm{W0}i}>\Delta P_{\mathrm{L}}$	$\sum_{i=1}^{N}\Delta P_{\mathrm{W0}i}h'_{\mathrm{step}}(t_{\mathrm{d}}^+-t_{\mathrm{d}})>\Delta P_{\mathrm{L}}h'_{\mathrm{step}}(t_{\mathrm{d}}^+)$

Furthermore, the characteristic analysis of $h'_{\mathrm{step}}(t)$ reveals that $h'_{\mathrm{step}}(t)$ exhibits the decreasing characteristic during a period after the zero-time instant, i. e., $h'_{\mathrm{step}}(t_{\mathrm{d}}^+-t_{\mathrm{d}})>h'_{\mathrm{step}}(t_{\mathrm{d}}^+)$. When WTs adopt identical TLIC parameters under both SIIS and SIDS, the latter will induce a more pronounced FR phenomenon. This conclusion aligns with the simulation results demonstrated in Fig. 6.

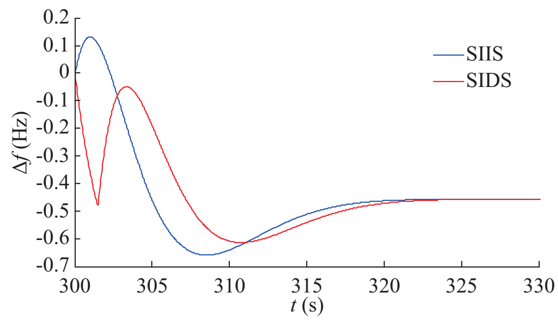

Fig. 6. Simulation results of Δf under SIIS and SIDS.

From the above results and analysis, it can be concluded that when all WTs simultaneously activate the TLIC method for frequency regulation, the WF power experiences a substantial increase, resulting in a reverse frequency surge. However, as the TLIC power maintains a continuous decreasing trend, the frequency subsequently declines. This indicates that the reverse frequency surge is unnecessary and adversely affects the subsequent frequency response process. Consequently, the effectiveness of WF participating in frequency regulation fails to achieve significant improvement.

IV. Multi-turbine Cooperative Frequency Regulation Control Method of WFs

Addressing the FR phenomenon discussed in Section III, this section first presents the analysis of frequency response under the sequential support (SQS). Building upon this foundation, a multi-turbine cooperative frequency regulation control method is proposed for WFs. This method aims to prevent the excessive electric power growth caused by simultaneous support and the resultant FR phenomenon.

A. Analysis of Frequency Response Under SQS

To simplify the derivation and analysis, two WTs employing the TLIC method are taken as a representative case. The specific scenarios are configured as follows.

1) Scenario 1: two WTs activate the TLIC method simultaneously and immediately.

2) Scenario 2: two WTs activate the TLIC method sequentially, where one is activated immediately and the other one is activated after t_{d}.

The time-domain frequency response forms in the two scenarios are obtained as:

$$\Delta f^{\mathrm{S1}}(t)=\Delta f_{\mathrm{W1}}^{\mathrm{S1}}(t)+\Delta f_{\mathrm{W2}}^{\mathrm{S1}}(t)-\Delta f_{\mathrm{L}}(t) \tag{22}$$

$$\Delta f^{\mathrm{S2}}(t)=\Delta f_{\mathrm{W1}}^{\mathrm{S2}}(t)+\Delta f_{\mathrm{W2}}^{\mathrm{S2}}(t)-\Delta f_{\mathrm{L}}(t) \tag{23}$$

where superscripts S1 and S2 represent scenarios 1 and 2, respectively.

By subtracting (23) from (22), the frequency response difference $\delta f(t)$ between the two scenarios is derived as:

$$\delta f(t)=\Delta f^{S2}(t)-\Delta f^{S1}(t)=\Delta f_{W2}^{S2}(t)-\Delta f_{W2}^{S1}(t) \tag{24}$$

Substituting (14) and (16) into (24), we have:

$$\begin{aligned}\delta f(t)=&\Delta P_{W0}\left(h_{step}(t-t_d)-h_{step}(t)\right)+\\&K_{P,t}\left(h_{ramp}(t-t_d)u(t-t_d)-h_{ramp}(t)u(t)\right)-\\&K_{P,t}\left(h_{ramp}(t-t_d-\tau)u(t-t_d-\tau)-h_{ramp}(t-\tau)u(t-\tau)\right)\end{aligned} \tag{25}$$

1) $0<t<t_d$

$$\delta f(t)=-\Delta P_{W0}h_{step}(t)-K_{P,t}h_{ramp}(t) \tag{26}$$

One WT has not activated TLIC method in scenario 2, which induces the larger frequency deviation, naturally $-\Delta P_{W0}h_{step}(t)-K_{P,t}h_{ramp}(t)<0$ and $\delta f(t)<0$. However, the frequency in this process would not reach the nadir, so this part mainly discusses the frequency response characteristics in the subsequent process.

2) $t_d<t<\tau$

$$\begin{aligned}\delta f(t)=&\Delta P_{W0}\left(h_{step}(t-t_d)-h_{step}(t)\right)+\\&K_{P,t}\left(h_{ramp}(t-t_d)-h_{ramp}(t)\right)\end{aligned} \tag{27}$$

Since $h_{ramp}(t)$ exhibits a monotonically increasing characteristic, $h_{ramp}(t-t_d)-h_{ramp}(t)<0$ and $K_{P,t}<0$. However, due to the continuity of $h_{step}(t-t_d)-h_{step}(t)$, $\delta f(t)$ within this time interval also demonstrates the characteristic of transitioning from negative to positive values.

3) $\tau<t<t_d+\tau$

$$\begin{aligned}\delta f(t)=&\Delta P_{W0}\left(h_{step}(t-t_d)-h_{step}(t)\right)+\\&K_{P,t}\left(h_{ramp}(t-t_d)-h_{ramp}(t)\right)+K_{P,t}h_{ramp}(t-\tau)\end{aligned} \tag{28}$$

Since $h_{step}(t)$ exhibits a decreasing characteristic, $\Delta P_{W0}\left(h_{step}(t-t_d)-h_{step}(t)\right)>0$. And $h_{ramp}(t)$ exhibits the approximate linear characteristic, as shown in Fig. 7, so $h_{ramp}(t-t_d)-h_{ramp}(t)\approx h_{ramp}(t_d)$. However, in this time interval, $h_{ramp}(t-\tau)>-h_{ramp}(t_d)$, so $\delta f(t)>0$.

4) $t>t_d+\tau$

$$\begin{aligned}\delta f(t)=&\Delta P_{W0}\left(h_{step}(t-t_d)-h_{step}(t)\right)+K_{P,t}\left(h_{ramp}(t-t_d)-\right.\\&\left.h_{ramp}(t)\right)-K_{P,t}\left(h_{ramp}(t-t_d-\tau)-h_{ramp}(t-\tau)\right)\end{aligned} \tag{29}$$

Similarly, $h_{ramp}(t)$ shows the approximate linear characteristic, so $h_{ramp}(t-t_d)-h_{ramp}(t)\approx h_{ramp}(t_d)$ and $h_{ramp}(t-t_d-\tau)-h_{ramp}(t-\tau)\approx h_{ramp}(t_d)$. The two effects cancel each other out, so $\Delta P_{W0}\left(h_{step}(t-t_d)-h_{step}(t)\right)\geq 0$ and $\delta f(t)\geq 0$ in this interval.

In summary, within the time interval $(t>\tau)$ when the FN is most likely to occur, the following relationship $\delta f(t)>0$ consistently holds. This indicates that compared with scenario 1 with simultaneous immediate TLIC method activation, scenario 2 employing sequential TLIC method activation of the two WTs demonstrates superior frequency response characteristics during this critical interval. Specifically, higher FN values are maintained and the enhanced frequency regulation performance is achieved.

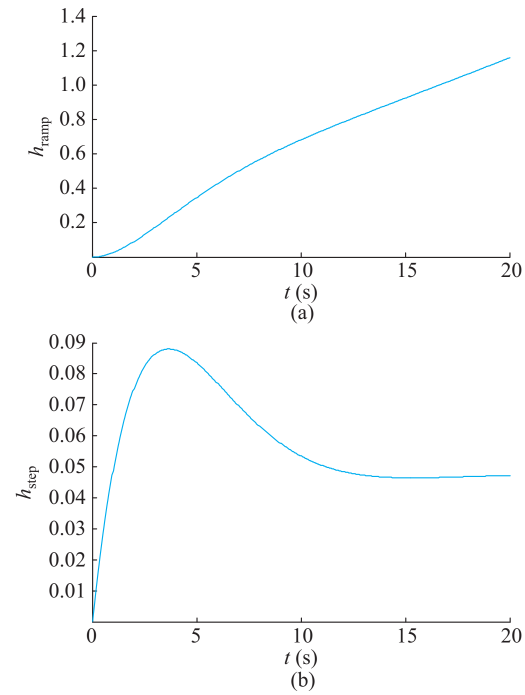

Fig. 7. Characteristic curves of h_{step} and h_{ramp}. (a) h_{step}. (b) h_{ramp}.

B. Multi-turbine Cooperative Frequency Regulation Control Method

For individual WTs, both MPPT and TLIC methods are implemented. During normal operation when no power support is required, the WT operates in the mode of MPPT method defined by (3). When the frequency regulation demands active power support, the WT switches to the mode of TLIC method governed by (1). The distinction between different WTs lies in their mode-switching timing sequences. This staggered transition mechanism constitutes the multi-turbine cooperative frequency regulation control method for WFs. The diagram and the flowchart of the proposed multi-turbine cooperative frequency regulation control method are illustrated in Figs. 8 and 9, respectively, where P_{ei} is the electromagnetic power command dispatched to the i^{th} WT; and Δf_{thd} is the threshold of frequency deviation.

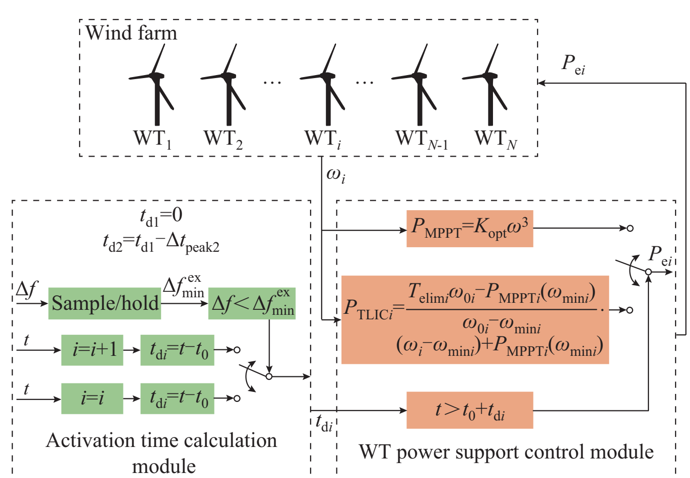

Fig. 8. Diagram of proposed multi-turbine cooperative frequency regulation control method.

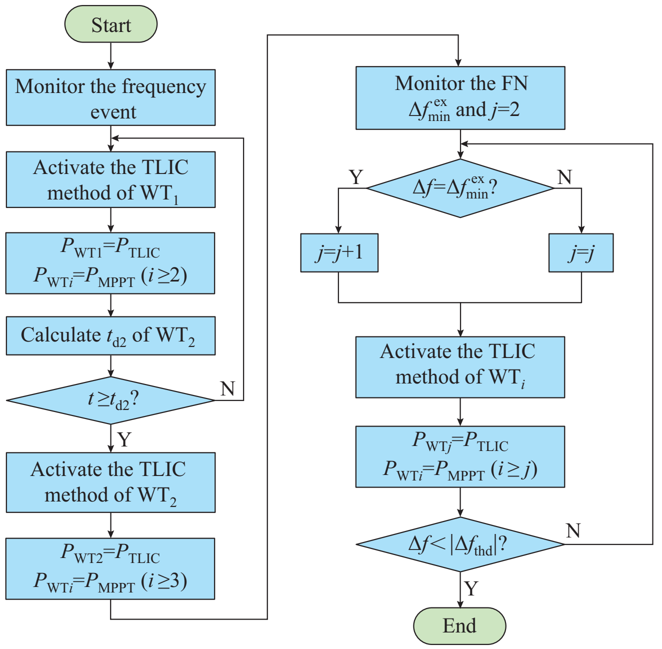

Fig. 9. Flowchart of proposed multi-turbine cooperative frequency regulation control method.

1) WT_1: activate the TLIC method immediately after the frequency event to provide power support, thereby suppressing the rapid frequency decline.

$$t_{d1}=0 \tag{30}$$

2) WT_2: based on the moment of the FN under load power disturbance, the activation timing of the TLIC method for WT_2 t_{d2} is estimated following the principle of maximizing its contribution to the frequency improvement at that moment, thereby enhancing the FN [16].

$$t_{d2}=\Delta t_{nadir}-\Delta t_{peak2} \tag{31}$$

where Δt_{peak2} is the peaking moment of the frequency response under the TLIC power of WT_2; and Δt_{nadir} is the occurring moment of the FN activated only by the load power.

3) WT_i ($i\geq 3$): the previous FN is recorded as Δf_{min}^{ex}. Whenever the frequency reaches this nadir, one of the remaining WTs not yet participating in frequency regulation is activated and switched from MPPT to TLIC.

$$t_{di}=\left\{t \,\middle|\, \Delta f(t)=\Delta f_{min}^{ex}\right\} \quad i\geq 3 \tag{32}$$

Since t_d is determined based on the frequency status information, it offers strong engineering practicality. In contrast, the proposed multi-turbine cooperative frequency regulation control method implements SQs of the TLIC method across WTs (denoted as proposed SQS hereafter).

Under the TLIC method, the electric power output of WTs progressively decreases over time. In the simultaneous support methods, all WTs synchronously increase and subsequently decrease their power output, which concentrates the frequency regulation energy from all WTs within a brief time window, while lacking additional WTs to compensate for the overall power decline in the WF. In contrast, the proposed cooperative multi-turbine frequency regulation control method implements sequential activation of the TLIC method across WTs. This method achieves two critical improvements: ① eliminate excessive power spikes caused by concurrent WT activation, and ② compensate the early-activated WTs experiencing power reduction. Thus, the adverse effect caused by the WF power reduction is mitigated, and the WF frequency regulation energy is distributed more uniformly over a longer period.

As the frequency regulation process progresses, the unbalanced power of the system decreases. Hence, in the earlier stage, WTs with high wind speed and large capacity first activate the TLIC method, followed subsequently by the WTs with lower wind speed and smaller capacity in the latter stage.

V. Simulation and Experiment Validation

A. Simulation Scenario Setup and Effectiveness Validation

In this subsection, the WF is equivalently aggregated into five WTs, with a wind power penetration rate of 25%. The frequency event triggered by a load surge of 300 kW occurs in the power system at 300 s. Two cases are established as follows. ① Case 1: five WTs share identical initial states (e.g., wind speed and rotor speed) with an initial wind speed of 10 m/s. ② Case 2: five WTs operate under different initial states with initial wind speeds of 10 m/s, 9 m/s, 8 m/s, 7 m/s, and 6 m/s, respectively.

The proposed SQS is compared with NoS, SIIS, and SIDS. Taking the wind power penetration rate of 25% as an example, the trajectories of Δf, P_W, P_M, and ΔP under NoS, SIIS, SIDS, and proposed SQS in Cases 1 and 2 are shown in Figs. 10 and 11, respectively; and the trajectories of ω and P_W of WTs under Cases 1 and 2 are shown in Figs. 12 and 13, respectively. Simulation results of FN under NoS, SIIS, SIDS, and proposed SQS are provided in Table II.

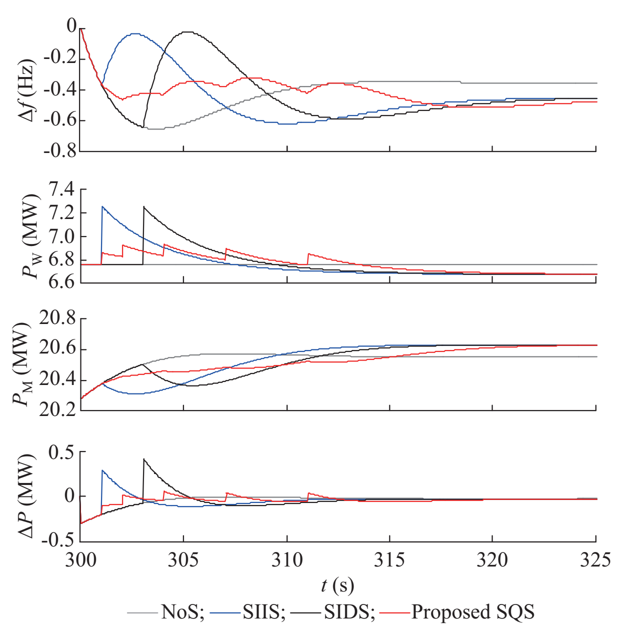

Fig. 10. Trajectories of Δf, P_W, P_M, and ΔP under NoS, SIIS, SIDS, and proposed SQS in Case 1 with wind power penetration of 25%.

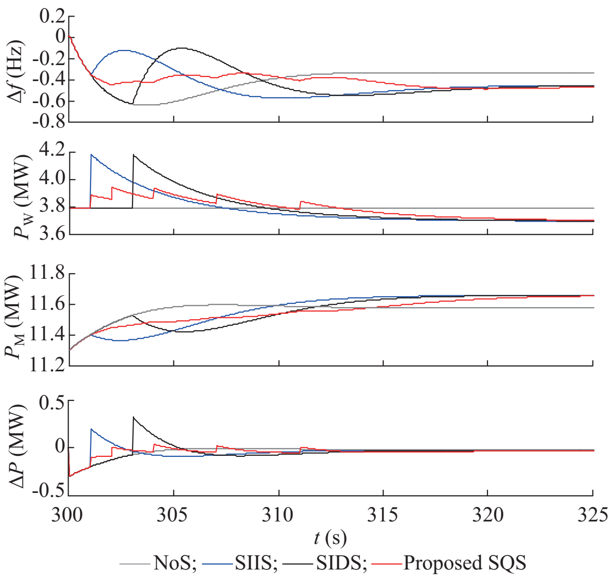

Fig. 11. Trajectories of Δf, P_W, P_M, and ΔP under NoS, SIIS, SIDS, and proposed SQS in Case 2 with wind power penetration of 25%.

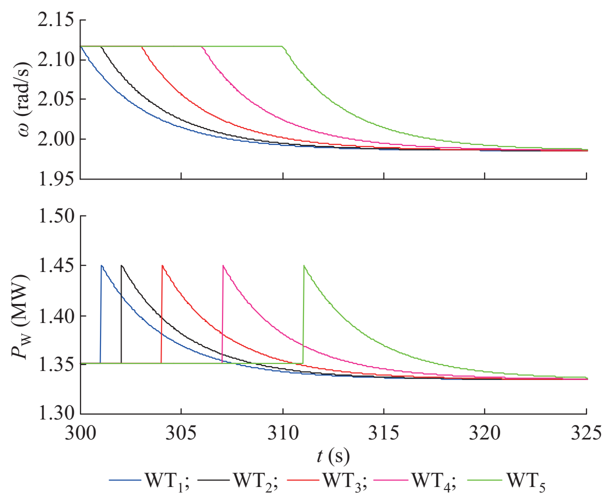

Fig. 12. Trajectories of ω and P_W of five WTs in Case 1 with wind power penetration of 25%.

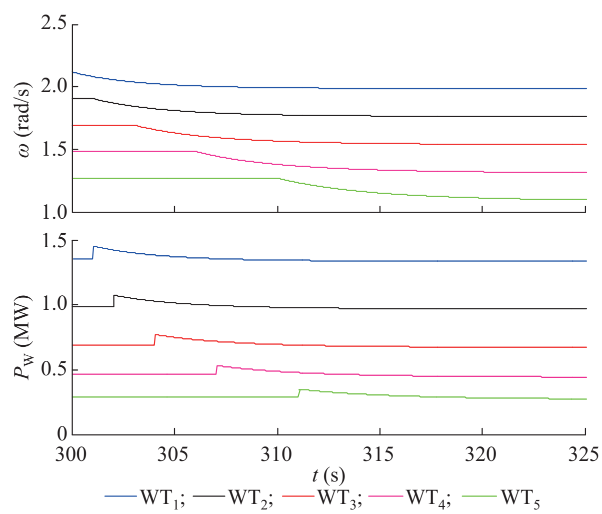

Fig. 13. Trajectories of ω and P_W of five WTs in Case 2 with wind power penetration of 25%.

TABLE II
SIMULATION RESULT OF FN UNDER NOS, SIIS, SIDS, AND PROPOSED SQS

Case	Penetration rate (%)	FN (Hz)			
		NoS	SIIS	SIDS	Proposed SQS
1	17	–0.8912	–0.8138	–0.7525	–0.6855
	25	–0.7731	–0.6914	–0.7554	–0.5757
	50	–0.6602	–0.6587	–0.6043	–0.5155
	77	–0.5607	–0.5845	–0.5428	–0.4569
2	17	–0.8637	–0.7635	–0.7357	–0.6308
	25	–0.7543	–0.6409	–0.7386	–0.5462
	50	–0.6434	–0.6075	–0.5571	–0.4859
	77	–0.5326	–0.5340	–0.4965	–0.4271

1) Case 1

After the load event occurs, if all WTs operate in the mode of MPPT method without providing power support, only the SGs increase the output, resulting in the FN of –0.6602 Hz. When all WTs participate in the frequency regulation using the TLIC method, the initial power increase from the WF exceeds the power imbalance in the system at the support moment, leading to a significant FR. However, this FR creates an illusion for the primary frequency regulation of SGs that rely on the frequency deviation as the control input. Instead of increasing the output power, the SGs reduce their output, directly affecting the FN and the recovery process.

In the case that all WTs activate the TLIC method simultaneously and immediately, the FN is –0.6587 Hz, which is similar to that under the MPPT method, limiting the effectiveness of wind power participating in the frequency regulation. When WTs delay the activation of the TLIC method to provide support, the FR at the support moment becomes more pronounced (as shown by the black curve in Fig. 10), with a corresponding FN of –0.6043 Hz.

For the proposed SQS, all WTs no longer activate the TLIC method simultaneously. Instead, the TLIC method are sequentially activated. Hence, the WF power no longer exhibits a significant sudden increase, and no FR occurs. Furthermore, unlike SIIS and SIDS, which concentrate on the frequency regulation energy within a short period, the proposed SQS distributes the frequency regulation energy more evenly over a longer period. By utilizing the TLIC power increments from newly activated WTs to compensate for the gradually decreasing power of earlier activated WTs, the abrupt surge and drop of the WF power injection into the grid are avoided. Accordingly, the FN under the proposed SQS is –0.5155 Hz, representing improvements of 21.9%, 21.7%, and 14.7%, compared with the aforementioned NoS, SIIS, and SIDS, respectively. This demonstrates that the proposed SQS achieves superior performance in suppressing FR and improving the FN.

2) Case 2

Unlike Case 1 where all WTs share identical initial operation states, Case 2 sets different initial operation states for WTs to better align with real-world conditions. The simulation results for Case 2 are similar to those of Case 1. When the WF does not participate in the frequency regulation, the FN is –0.6434 Hz. When all WTs immediately activate the TLIC method to provide power support, the FN is –0.6075 Hz. And for the case where all WTs delay TLIC method activation, the FN is –0.5571 Hz. When the WF adopts the proposed SQS, the FN is further improved to –0.4859 Hz.

A simulation model is established considering different communication delays. These delays directly changes the time-domain format of the WF power, and further affects the FNs. It is worth noting that the communication delay makes the least influence on the proposed SQS. Moreover, the proposed SQS has the strong robustness under various wind power penetration rates.

B. Test Bench Introduction and Result Analysis

1) Test Bench of Power System Integrating Wind Power

The test bench includes three WT simulators (WTSs) [35], [36], an SG simulator (SGS), and a feedback load (FL). The test bench structure is shown in Supplementary Material A Fig. SA1, with key parameters listed in Table III. Due to the decoupled control of active and reactive power, this paper mainly focuses on the impact of active power control on the frequency dynamics, while the reactive power and voltage control are not discussed. The experimental grid voltage is regulated to 380 V via the excitation voltage regulator of the SG.

TABLE III
KEY PARAMETERS OF TEST BENCH

Unit	Parameter	Value
WTS	Rated power (kW)	5.5
	Rated voltage (V)	380
	Rated frequency (Hz)	50
	Rated rotor speed (rad/s)	157.05
SGS	Rated power (kW)	6
	Rated voltage (V)	380
	Rated frequency (Hz)	50
	Rated rotor speed (rad/s)	157.05
FL	Rated power (kVA)	9
	Rated frequency (Hz)	50

1) WTS. Using algorithms such as power scaling, aeroelastic coupling characteristic simulation, inertia compensation, and damping compensation, the WTS with small capacity and low inertia can replicate the aerodynamic and slow dynamics of real WTs with large capacity and high inertia. The rotor-side converter receives the torque command calculated by the TLIC method and controls the generator to output the corresponding power for the short-term frequency support.

2) SGS. By employing inertia compensation, prime mover, and governor simulation algorithms, the SGS mimics mechanical dynamics and frequency response characteristics of the real SG. The prime mover and governor simulation algorithms compute mechanical torque based on the frequency sent to the drive converter to regulate the prime mover output.

3) FL. In the experimental grid, the FL simulates load variation characteristics. The rectifier consumes electric power from the WTSs and SGS in the experimental grid, while the inverter converts the power into a form acceptable to the public grid and feeds it back.

The data in the experimental platform, e.g., the WTS generator speed and output power, the SGS generator speed and output power, and the load power, are monitored and obtained by encoders and converter acquisition devices. These data are uploaded to a programmable logic controller (PLC) and a computer. Additionally, the proposed SQS for WTs and WF are implemented via PLC programming.

2) Experimental Result Analysis

The experiments are conducted with different wind power penetration rates of 19.4%, 44.8%, 63.0%, and 74.4%, respectively. The experimental results of FN under NoS, SIIS, SIDS, and proposed SQS are listed in Table IV, and the trajectories of Δf, P_W, and P_M under NoS, SIIS, SIDS, and proposed SQS with wind power penetration rate of 63.0% are shown in Fig. 14. Trajectories of ω and P_W of three WTs with wind power penetration rate of 63.0% are shown in Fig. 15. The wind speeds of three WTs are set to be 10 m/s, 9 m/s, and 8 m/s, respectively. The frequency event triggered by a load surge of 1.2 kW occurs at 300 s.

TABLE IV
EXPERIMENTAL RESULTS OF FN UNDER NOS, SIIS, SIDS, AND PROPOSED SQS

Penetration rate (%)	FN (Hz)			
	NoS	SIIS	SIDS	Proposed SQS
19.4	–0.7612	–0.6788	–0.6478	–0.5956
44.8	–0.8149	–0.6967	–0.6715	–0.6121
63.0	–0.8154	–0.6901	–0.6658	–0.6060
74.4	–0.8687	–0.7030	–0.6733	–0.6194

As shown in Figs. 14 and 15 and Table IV, the proposed SQS has the superior frequency regulation performance with different wind power penetration rates. Taking the penetration rate of 63.0% as an example, the WF exhibits the worst FN of –0.8154 Hz when not participating in the frequency regulation. Under the SIIS and SIDS, the WF power increment at the moment of TLIC method activation exceeds the system power deficit, resulting in the significant FR. This FR limits the output of SG and directly affects the subsequent frequency recovery process with the corresponding FN of –0.6901 Hz under SIIS and FN of –0.6658 Hz under SIDS, respectively.

In the proposed SQS, all WTs no longer activate the TLIC method simultaneously. This avoids abrupt power surges and FR, distributes the WF frequency regulation energy more evenly over a longer period, and elevates the FN to –0.6060 Hz, further improving the WF frequency regulation performance. Notably, the proposed SQS achieves these enhancements solely by adjusting the activation timing of the TLIC method, without compromising the dynamic stability of the WTs.

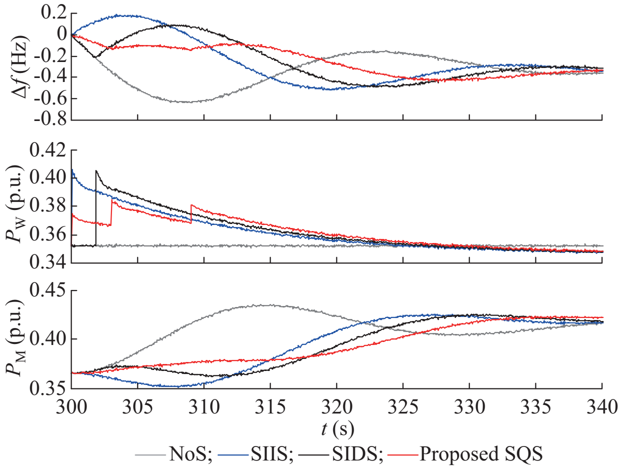

Fig. 14. Trajectories of Δf, P_W, and P_M under NoS, SIIS, SIDS, and proposed SQS with wind power penetration rate of 63.0%.

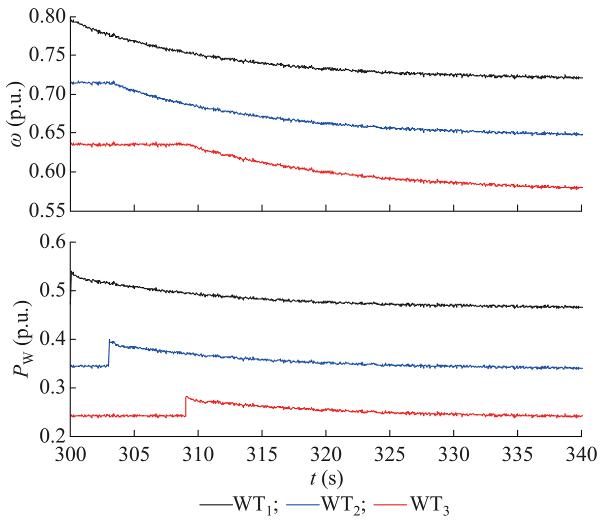

Fig. 15. Trajectories of ω and P_W of three WTs with wind power penetration rate of 63.0%.

VI. Conclusion

After the frequency events such as sudden load increases, all WTs in WF clusters simultaneously boost power generation to provide active power support. However, the resulting power increment exceeds the system power deficit, inducing the FR phenomenon. This phenomenon not only proves unnecessary but also creates a false perception of power surplus for SGs, consequently constraining their power ramping capabilities and adversely affecting both the FN and restoration process. To address these challenges, this paper focuses on the TLIC method, which is recognized for its superior rotor speed stability and absence of SFD issues. The occurrence conditions for FR are first derived under the SIIS and SIDS. Then, a multi-turbine cooperative frequency regulation control method is developed, incorporating TLIC power characteristics. By continuously monitoring the frequency dynamic and detecting recurrence of previous FNs, the proposed SQS implements the sequential activation of TLIC across WTs, mitigates excessive power increments from simultaneous support and compensates for electric power reduction of already activated WTs. The proposed SQS effectively suppresses power surges and drops inherent to concurrent support, thereby achieving significant FR suppression and FN elevation. In the future work, the cooperative perspective will be expanded to the coordination among different types of WTs. For example, in the far offshore WF, the coordination between the grid-forming and grid-following WTs needs to be discussed.

References

[1] EIA. (2023, Jan.). Electricity generation from wind. [Online]. Available: https://www. eia. gov/energyexplained/wind/electricity-generation-fromwind.php.

[2] US Department of Energy. (2023, Feb.). How wind energy became integral to the modern grid. [Online]. Available: https://www.energy.gov/eere/wind/articles/how-wind-energybecame-integral-modern-grid.

[3] R. Wang, S. Qin, W. Bao *et al.*, "Configuration and control strategy for an integrated system of wind turbine generator and supercapacitor to provide frequency support," *International Journal of Electrical Power and Energy Systems*, vol. 154, p. 109456, Dec. 2023.

[4] Q. Meng, J. Xu, L. Ge *et al.*, "Economic optimization operation approach of integrated energy system considering wind power consumption and flexible load regulation," *Journal of Electrical Engineering and Technology*, vol. 19, no. 1, pp. 209-221, Jul. 2024.

[5] H. Liu, X. Peng, C. Zhang *et al.*, "Overview of wind power participating in frequency regulation control strategy for power system," *Electric Power Automation Equipment*, vol. 41, no. 11, pp. 81-92, Nov. 2021.

[6] *Wind Farm Access to the Power System Technical Regulations*. GB/T 19963-2021.

[7] J. Zhang, B. Zhang, Q. Li *et al.*, "Fast frequency regulation method for power system with two-stage photovoltaic plants," *IEEE Transactions on Sustainable Energy*, vol. 13, no. 3, pp. 1779-1789, Jul. 2022.

[8] S. Wang and K. Tomsovic, "Fast frequency support from wind turbine generators with auxiliary dynamic demand control," *IEEE Transactions on Power Systems*, vol. 34, no. 5, pp. 3340-3348, Sept. 2019.

[9] P. Keung, P. Li, H. Banakar *et al.*, "Kinetic energy of wind turbine generators for system frequency support," *IEEE Transactions on Power Systems*, vol. 24, no. 1, pp. 279-287, Feb. 2009.

[10] C. Zhao, D. Sun, X. Zhang *et al.*, "A two-stage power distribution scheme of multiple wind farms participating in primary frequency regulation," *IEEE Transactions on Power Systems*, vol. 38, no. 6, pp. 5009-5021, Nov. 2023.

[11] J. V. Vyver, D. M. D. Kooning, B. Meersman *et al.*, "Droop control as an alternative inertial response strategy for the synthetic inertia on wind turbines," *IEEE Transactions on Power Systems*, vol. 31, no. 2, pp. 1129-1138, Mar. 2016.

[12] W. Bao, L. Ding, Z. Liu *et al.*, "Analytically derived fixed termination time for stepwise inertial control of wind turbines–part I: analytical derivation," *International Journal of Electrical Power and Energy Systems*, vol. 121, p. 106120, Oct. 2020.

[13] M. Kheshti, L. Ding, W. Bao *et al.*, "Toward intelligent inertial frequency participation of wind farms for the grid frequency control," *IEEE Transactions on Industrial Informatics*, vol. 16, no. 11, pp. 6772-6786, Nov. 2020.

[14] Y. Li, Q. Li, Z. Chen *et al.*, "Maximum-frequency-deviation-oriented optimal short-term frequency support strategy of wind turbines and the mechanism," *Proceedings of the CSEE*, vol. 44, no. 3, pp. 1020-1034, Feb. 2024.

[15] M. Sun, F. Xu, L. Chen *et al.*, "Optimal auxiliary frequency control strategy of wind turbine generator utilizing rotor kinetic energy," *Proceedings of the CSEE*, vol. 41, no. 2, pp. 506-513, Jan. 2021.

[16] W. Gu, Z. Chen, Q. Li *et al.*, "Torque limit-based inertial control method based on delayed support for primary frequency control of wind turbines," *Journal of Modern Power Systems and Clean Energy*, vol. 12, no. 2, pp. 561-570, Mar. 2024.

[17] M. Kang, K. Kim, E. Muljadi *et al.*, "Frequency control support of a doubly-fed induction generator based on the torque limit," *IEEE Transactions on Power Systems*, vol. 31, no. 6, pp. 4575-4583, Nov. 2016.

[18] J. Zhao, M. Li, X. He *et al.*, "Coordinated control strategy of wind power and energy storage in frequency regulation based on torque limit control," *Transactions of China Electrotechnical Society*, vol. 34, no. 23, pp. 4982-4990, Dec. 2019.

[19] S. Ma, H. Geng, G. Yang *et al*., "Virtual inertia control of variable-speed wind turbines based on the switching of power point tracking curves," *Automation of Electrical Power Systems*, vol. 42, no. 17, pp. 42-48, Sept. 2018.

[20] M. Kheshti, S. Lin, X. Zhao *et al*., "Gaussian distribution-based inertial control of wind turbine generators for fast frequency response in low inertia systems," *IEEE Transactions on Sustainable Energy*, vol. 13, no. 3, pp. 1641-1653, Jul. 2022.

[21] Z. Huang, W. Wu, C. Lin *et al*., "Cooperative strategies for frequency control of wind turbines to mitigate secondary frequency dip: coefficient allocation and exit techniques," *IEEE Transactions on Sustainable Energy*, vol. 16, no. 2, pp. 1056-1067, Apr. 2025.

[22] X. Lyu, Y. Jia, and Z. Y. Dong, "Adaptive frequency responsive control for wind farm considering wake interaction," *Journal of Modern Power Systems and Clean Energy*, vol. 9, no. 5, pp. 1066-1075, Sept. 2021.

[23] Z. Wang, J. Liu, G. Li *et al*., "Droop-inertia frequency regulation feasible region assessment for wind farm based on data-driven state space mapping," *IEEE Transactions on Industry Applications*, vol. 61, no. 1, pp. 1704-1715, Jan. 2025.

[24] T. He, L. Sun, C. Wang *et al*., "A method of primary frequency regulation power distribution in a wind farm to avoid secondary frequency drop," *Power System Protection and Control*, vol. 50, no. 11, pp. 12-20, Jun. 2022.

[25] S. Li, W. Wang, X. Zhang *et al*., "A novel primary frequency regulation strategy of wind farm based on wind turbine health condition," *IET Renewable Power Generation*, vol. 16, pp. 2101-2110, May 2022.

[26] Z. Guo and W. Wu, "Data-driven model predictive control method for wind farms to provide frequency support," *IEEE Transactions on Energy Conversion*, vol. 37, no. 2, pp. 1304-1313, Jun. 2022.

[27] Y. Chen, G. Wang, Q. Shi *et al.*, "A new coordinated virtual inertia control strategy for wind farms," *Automation of Electrical Power Systems*, vol. 39, no. 5, pp. 27-33, Mar. 2015.

[28] Q. Shi, G. Wang, H. Li *et al.*, "Coordinated virtual inertia control strategy of multiple wind turbines in wind farms considering frequency regulation capability," *Power System Technology*, vol. 43, no. 11, pp. 4005-4015, Nov. 2019.

[29] X. Ji, K. Jiang, Y. Yao *et al*., "Frequency collaborative support control of wind farm considering operation state difference of wind turbines," *Electric Power Automation Equipment*, vol. 44, no. 3, pp. 98-104, Mar. 2024.

[30] K. Liu, Y. Qu, H. Kim *et al*., "Avoiding frequency second dip in power unreserved control during wind power rotational speed recovery," *IEEE Transactions on Power Systems*, vol. 33, no. 3, pp. 3097-3106, May 2018.

[31] T. Jiang, Y. Qiu, X. Liu *et al*., "Control strategy with dynamic and differentiated timing synergy for multiple wind farms supporting frequency stability of power grid," *Automation of Electrical Power Systems*, vol. 48, no. 8, pp. 162-173, Apr. 2024.

[32] H. Lao, L. Zhang, T. Zhao *et al.*, "Frequency regulation strategy for wind power considering grouping control and orderly recovery," *Automation of Electrical Power Systems*, vol. 44, no. 16, pp. 114-120, Aug. 2020.

[33] B. Boukhezzar and H. Siguerdidjane, "Nonlinear control of a variable-speed wind turbine using a two-mass model," *IEEE Transactions on Energy Conversion*, vol. 26, no. 1, pp. 149-162, Mar. 2011.

[34] P. M. Anderson and M. Mirheydar, "A low-order system frequency response model," *IEEE Transactions on Power Systems*, vol. 5, no. 3, pp. 720-729, Aug. 1990.

[35] M. Yin, W. Li, C. Y. Chung *et al.*, "Inertia compensation scheme of WTS considering time delay for emulating large-inertia turbines," *IET Renewable Power Generation*, vol. 11, no. 4, pp. 529-538, Mar. 2017.

[36] W. Li, M. Yin, Z. Chen *et al.*, "Inertia compensation scheme for wind turbine simulator based on deviation mitigation," *Journal of Modern Power Systems and Clean Energy*, vol. 5, no. 2, pp. 228-238, Mar. 2017.

Wei Gu received the B.Eng. degree in electrical power engineering and the Ph.D. degree in control science and engineering from Nanjing University of Science and Technology, Nanjing, China, in 2017 and 2023, respectively. He is currently working in School of Automation, Nanjing University of Science and Technology, Nanjing, China. His research interests include active power control of wind turbine, and frequency stability control of power system.

Minghui Yin received the B.Eng. and M.Eng. degrees in electrical power engineering and the Ph.D. degree in control science and engineering from Nanjing University of Science and Technology, Nanjing, China, in 1999, 2002, and 2009, respectively. He is currently working as a Professor in School of Automation, Nanjing University of Science and Technology. His research interests include wind power system design and control, and power system stability operation and control.

Qiang Li received the B.Eng., M.Eng., and Ph.D. degrees in power systems and automation from Hohai University, Nanjing, China, in 2003, 2006, and 2011, respectively. He is currently a Professorate Senior Engineer with the State Grid Jiangsu Electric Power Co., Ltd. Research Institute, Nanjing, China. His research interest includes flexible transmission of mid-to-far offshore wind power.

Yaran Li received the B.Eng degree in electrical power engineering from Southeast University, Nanjing, China, in 2017, and the Ph.D. degree in electrical power engineering from The University of New South Wales, Sydney, Australia, in 2021, respectively. She is currently working in the State Grid Jiangsu Electric Power Co., Ltd. Research Institute, Nanjing, China. Her research interests include offshore wind power integration and control technology.

Zaiyu Chen received the B.S. and Ph.D. degrees from Nanjing University of Science and Technology, Nanjing, China, in 2012 and 2019, respectively. He was a Research Fellow with the School of Electrical and Electronic Engineering, Nanyang Technological University, Singapore, from Jan. 2020 to Mar. 2021. He is currently working in School of Automation, Nanjing University of Science and Technology. His research interests include active power control of wind turbine and its application in power system frequency regulation.

Qun Li received the B.Eng. degree in electronic equipment structure design from Southeast University, Nanjing, China, in 1989, the M.Eng. degree in electronic equipment structure design from Xidian University, Xi'an, China, in 1995, and the Ph.D. degree in power systems and automation from Southeast University, in 1999, respectively. He is currently a Professorate Senior Engineer with the State Grid Jiangsu Electric Power Co., Ltd. Research Institute, Nanjing, China. His research interests include power quality analysis and renewable power integration.